PROCEEDINGS OF SCIENCE

Long-term evolution of nonthermal emission from various types of supernova remnants in a diversified circumstellar medium

Ryosuke Kobashi,[a,*] **Haruo Yasuda**[a] **and Shiu-Hang Lee**[a,b]

[a] *Department of Astronomy, Kyoto University, Kitashirakawa, Oiwake-cho, Sakyo-ku, Kyoto 606-8502, Japan*

[b] *Kavli Institute for the Physics and Mathematics of the Universe (WPI), The University of Tokyo, Kashiwa 277-8583, Japan*

E-mail: kobashi@kusastro.kyoto-u.ac.jp

The contribution of galactic supernova remnants (SNRs) to the origin of cosmic rays (CRs) remains an important open question in modern astrophysics. Because CRs generated in SNRs will interact with dense circumstellar material (CSM) or molecular clouds and then utter non-thermal emission, non-thermal emission from SNRs can bring us energy budget and production history of CRs in SNRs. We perform hydrodynamic simulations to model the long-term SNR evolution from explosion all the way to the radiative phase (or 300,000 yr at maximum) by using CR-Hydro code developed by previous work and compute the time evolution of the broadband nonthermal spectrum. We assume uniform density media for the ambient environment of Type Ia SNRs and constant mass loss rate with outer uniform density for core-collapse SNRs, created by the stellar wind of a massive red supergiant star. Our results from a parametric study of environment density reveal a highly diverse evolution history of the nonthermal emission closely correlated to the environmental characteristics of an SNR. Up to the radiative phase, the effects of CR reacceleration and ion-neutral wave damping are studied. More detailed discussions or an assessment of the next-generation telescope mission in X-ray band *JEDI* (which is referred as *FORCE* in the paper) are found in [1].

38th International Cosmic Ray Conference (ICRC2023)
26 July - 3 August, 2023
Nagoya, Japan

*Speaker

PoS(ICRC2023)878

1. Introduction

Towards understanding the contribution of supernova remnants (SNRs) to the production of Galactic cosmic rays (CRs), it is important to follow the production history of CRs in a SNR throughout its lifetime. Observationally, non-thermal emission across a wide energy range provides us the inference of CR production in a SNR. The diverse interstellar medium (ISM) and circumstellar medium (CSM) surrounding the SNRs are known to be one of the most important determining factors for the CR acceleration history and hence the resulted time evolution of the non-thermal emission (e.g., [2, 3]). Comparisons of hydrodynamic models with observational data have been performed for individual SNRs to estimate their CR energy budgets (e.g., [4, 5]). However, systematic parametric surveys covering the rich diversity of the ambient environments and progenitors of various types of SNRs are still absent.

The CR acceleration efficiency and thus the current amount of CR produced in a SNR strongly depends on the ambient environment and age as well as the progenitor system. Therefore, it is crucial to quantify the effects of environmental parameters such as the ambient gas density and magnetic field profiles with a self-consistent numerical setup. Indeed, [6] performed such a task up to a SNR age of 5,000 yrs, and found a rich variety of non-thermal emission evolution under different parameters for the surrounding environments. This result also in turn infers the ability of non-thermal emission observations on constraining the CSM structure and hence the pre-SN mass-loss activities of SN progenitors.

In this study, we extend the work by [6] to follow the evolution all the way from explosion to an age of a few 10^4 to 3×10^5 yrs, as well as the implementation of more realistic CSM environments for a red supergiant (RSG) star by performing a hydrodynamic simulation for the pre-SN wind-ISM interaction. We simulate the shock hydrodynamics and CR acceleration simultaneously until the forward shocks have weakened enough to stop accelerating CRs efficiently, i.e., up to an age of $\sim$ a few or tens of 10^4 yrs depending on the ejecta/CSM model. The resulted grid of SNR/CSM models will provide a broader vision on the long-term evolution of non-thermal emissions from SNRs interacting with different kinds of environments.

A novel aspect introduced in this work is the self-consistent inclusion of the radiative phase of a SNR inside a CR-hydrodynamic simulation framework. Middle-aged SNRs bright in radio and gamma-ray such as W44 and IC 443 (e.g., [7]) are usually found to possess radiative shocks. Their bright radio synchrotron emission and GeV gamma-rays from π^0-decay are suggested to originate from a rapid compression of gas, CRs and magnetic field in the cold dense shell formed behind the radiative shocks (e.g., [8]). Moreover in the radiative phase, it has been suggested that re-acceleration of pre-existing CRs (e.g., [9]) and the effects of ion-neutral damping of CR-trapping magnetic waves (e.g., [10, 11]) neraly account for the observed spectral properties in evolved SNRs. From the view point of better understanding the connection between the non-thermal emission properties of young and evolved SNRs, it is important to understand the role of re-acceleration of pre-existing CRs as a function of age under different ambient environment settings in our framework. In addition, a few other previous theoretical studies have also investigated the evolution of CR energetics as a function of SNR age (e.g., [12]), but these works primarily focused on the younger remnants with no discussion on the later evolution stages. Our study addresses these points using a coherent hydrodynamic simulation to connect the youngs to the olds. In this study, using

our grid of SNR/CSM models from explosion up to the radiative phase, we quantify the importance of CR re-acceleration in terms of the total CR energy budget throughout the lifetime of a SNR.

2. Simulation setup

2.1 Included physics

We use the *CR-Hydro* code developed by [6] with adaptations to fit the purposes of this work. The *CR-Hydro* code performs 1-D spherically symmetric hydro simulations on a Lagrangian grid *VH-1* (e.g., [13]) coupled with a semi-analytic non-linear diffusive shock acceleration (NLDSA) calculation (e.g., [14–16]) similar to the framework introduced in e.g., [12]. For radiative cooling, we adopt the non-equilibrium (NEQ) cooling function from [17] coupled to the exact time integration method of [18].

To obtain the phase-space distribution function of the accelerated protons $f(x,p)$, we solve the diffusion-convection equation in the shock rest frame (e.g., [12, 14–16]). From the formulation of the solution $f(x,p)$ [12, Eq.13], we can decompose it into two components depending on the type of seed particles being accelerated from:

$$\begin{aligned} f(x,p) \quad &\propto \quad \left[\frac{\eta n_0}{4\pi p_{\rm inj}^3}\exp\left(-\int_{p_{\rm inj}}^{p}\frac{dp'}{p'}\frac{3S_{\rm tot}U(p')}{S_{\rm tot}U(p')-1}\right)\right] \\ &+ \quad \int_{p_{\rm inj}}^{p}\frac{dp''}{p''}f_{\rm pre,p}(p'')\left[\exp\left(-\int_{p''}^{p}\frac{dp'}{p'}\frac{3S_{\rm tot}U(p')}{S_{\rm tot}U(p')-1}\right)\right], \end{aligned} \tag{1}$$

where $S_{\rm tot}$ is the effective total compression ratio of the shock, $U(p)$ is the dimensionless gas flow velocity, $f_{\rm pre,p}$ is the distribution function of any pre-existing CR protons. It has been suggested that re-acceleration of pre-existing CRs plays a pivotal role in the production of non-thermal emission in older SNRs [8, 9]. We will further elaborate in section 3.1 on the mechanism in detail. Following [8, 9], we assume that such pre-existing CRs $f_{\rm pre,p/e}$ are attributed to the Galactic CR protons and electrons+positrons.

The non-thermal emission is calculated and analyzed simultaneously in [1]. We do not consider the contribution from secondary particles produced through $\pi^{\pm}$ decays in this work, which can be important for very dense environments such as giant molecular clouds (see e.g., [8]) but is out of the scope of this work.

2.2 Model environment

We have prepared models in two categories, i.e., Group A (A1 – A3) and Group B (B1 – B5), for the circumstellar environments surrounding the SNR. For the models in Group A, we assume a uniform ambient medium with a constant gas density. This density $n_{\rm ISM}$ is varied over 10^{-3} cm^{-3}, 0.1 cm^{-3}, 10 cm^{-3}. In Group B, we consider the structure created by the progenitor stellar wind with a constant mass-loss rate blowing into a uniform medium. A wind bubble/shell is formed around the ejecta surrounded by a uniform ISM-like gas. The CSM structure is obtained by hydrodynamic simulations using the VH-1 code (e.g., [13]) with radiative loss taken into account [17]. The pre-SN CSM density profiles are plotted in Figure 1. The density of the wind deviates from a pure power-law r^{-2} near the interface with the outer ISM whose structure depends on the

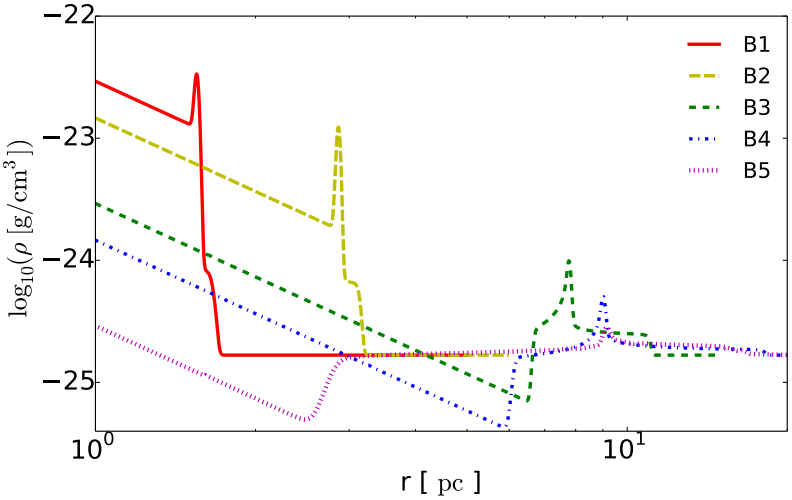

Figure 1: Radial density profiles of the ambient environments in the models of Group B. The red solid, yellow long-dashed, green dashed, blue dash-dotted and magenta dotted lines are associated with models B1, B2, B3, B4 and B5, of which the mass-loss rates of the progenitor are $\dot{M} = 10^{-4}, 5.0\times10^{-5}, 10^{-5}, 5.0\times10^{-6}, 10^{-6}$ $\mathrm{M_\odot/yr}$, respectively. The total mass-loss is 8 $\mathrm{M_\odot}$ for each model, and the gas density in the outer region is fixed at $n_{\mathrm{ISM}} = 0.1$ $\mathrm{cm^{-3}}$.The figure is taken from [1].

mass-loss rate. While the ejecta (progenitor) mass and the pre-SN mass-loss history are related to each other from stellar evolution models, we fix the ejecta mass in this study within each Group and vary the mass-loss rates $\dot{M} = 10^{-6} - 10^{-4}$ $\mathrm{M_\odot/yr}$ to study the effect of the latter on the SNR evolution. In the free-expanding wind, $\rho(r) = \dot{M}/(4\pi r^2 v_w)$ with the wind velocity assumed to be $v_w = 20$ km/s for a RSG star. The density of the outer uniform medium is fixed at $n_{\mathrm{ISM}} = 0.1$ $\mathrm{cm^{-3}}$. The magnetic field strength in the wind is determined by the magnetization parameter $\sigma_{\mathrm{w}} \equiv (B^2/8\pi)/(\rho v_{\mathrm{w}}^2/2) = 10^{-2}$ (e.g., [4, 12]). The magnetic field strength in the ISM-like ambient medium for models in both Groups A and B are on the other hand determined by scaling as proportional to $\sqrt{n_{\mathrm{ISM}}}$ assuming magnetic flux freezing under isothermal condition (e.g., [9, 24]). For $n_{\mathrm{ISM}} = 0.1$ $\mathrm{cm^{-3}}$ and $T_{\mathrm{ISM}} = 10^4$ K, we assume $B_{\mathrm{ISM}} = 1$ μG.

We can further categorize the initial CSM profiles into two types: B1–B2 and B3–B5. Models B1 and B2 have relatively large mass-loss rates which result in a dense wind shell whose spatial scale is mainly dictated by the mass loss duration prior to explosion. Models B3–B5 on the other hand form a wind "bubble" surrounded by a dense shell whose dynamics is determined by mechanical (pressure) balance instead. B5 in particular has a relatively small cavity-like structure due to the low mass-loss rate and hence gas ram pressure. The total mass-loss is fixed at 8 $\mathrm{M_\odot}$ for all models in Group B (see below). These differences in the CSM profiles will reflect strongly in the resulted light curves in the SNR phase.

We assume an ejecta with energetics typical of a Type Ia SN for Group A, and an ejecta from the core collapse (CC) explosion of a RSG star for Group B. We use the *DDT12* model [25, and references therein] for the Type Ia ejecta which is representative of a "normal" thermonuclear explosion of a near-Chandrasekhar mass white dwarf star, i.e., $M_{\mathrm{ej}} = 1.4$ $\mathrm{M_\odot}$, $E_{\mathrm{SN}} = 1.18\times10^{51}$ erg with an exponential profile [26]. A RSG model *s25D* [27, 28] is used for the CC SNRs in Group

B with an original ZAMS mass of 25 $M_\odot$, for which $M_{\rm ej}$ = 12.2 $M_\odot$, $E_{\rm SN} = 1.21 \times 10^{51}$ erg with a power-law envelope model [29] whose index is $n_{\rm pl}$ = 12 [30] for the ejecta density profile. This model involves a total mass-loss of 8 $M_\odot$ through stellar wind prior to CC. We fix $B_{\rm ej} = 10^{-7}$ G for the magnetic field in the ejecta in both groups which does not play much role in our results in this work.

3. Results

Here we present results showing the impact of physical processes in the radiative phase on the calculated emission spectra.

3.1 Re-acceleration effect

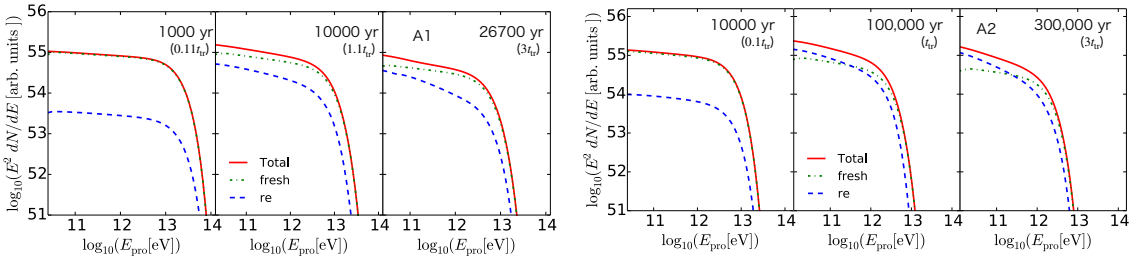

Figure 2: Time snapshots of CR proton spectra at three different dynamical ages integrated over the whole SNR volume for models A1 (left) and A2(right). The total spectra (red solid) is decomposed into components from the freshly accelerated CRs (green dashed-dotted) and the re-accelerated CRs (blue dashed-dotted) to visualize their relative contributions to the accelerated CRs. The plotted ages are chosen based on the transition time $t_{\rm tr}$ (The definition can be found in [1]). The figures are taken from [1].

As the SNR shock decelerates and eventually becomes radiative, the ability of the shock in injecting and accelerating thermal particles becomes weak. On the other hand, it has been shown that re-acceleration of pre-existing relativistic particles such as the Galactic CRs can remain effective at fast radiative shocks, which can take over as the dominant mechanism of non-thermal emission in more evolved SNRs. This effect from re-acceleration of pre-existing CRs in older SNRs with shock-cloud interactions have been investigated by a few recent works [e.g., 8, 9, 31, and reference therein], which suggest that the bright GeV gamma-ray and radio emission observed in middle-aged SNRs such as W44 and IC 443 can be mostly accounted for by the re-acceleration of Galactic CRs at their fast radiative cloud shock. These studies, however, initialized the cloud shock in an ad-hoc manner without considering the dynamics of the ejecta from explosion as well as in the earlier evolutionary stages before the SNR hits a dense cloud. This may lead to a failure in capturing the effects from the long-term evolution of the SNR and the complete history of CR acceleration from explosion to the current day. By including the essential physics similar to these previous works, our long-term simulations can serve to remedy this problem.

Based on [9], we take into account the re-acceleration of pre-existing cosmic rays in parallel to the injection of thermal particles in the DSA process throughout the whole lifetime of a SNR until its shock dies out. In addition, by adding this effect to our self-consistent calculations, we can more

accurately estimate the total amount of CRs accelerated through the lifetime of a SNR, thus helping us evaluate quantitatively the contribution of re-acceleration to the total CR output from a remnant as a function of age.

3.2 CR production history

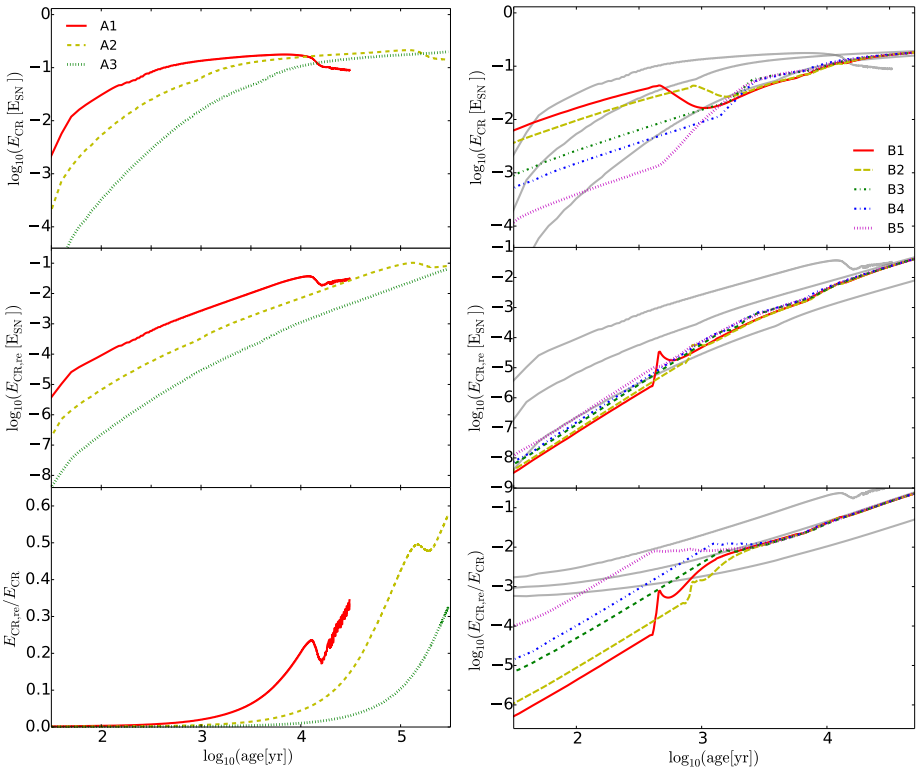

Figure 3: Left panel: The total kinetic energy in the accelerated CRs integrated over the SNR volume as a function of age for models A1 to A3. The line in red solid, in yellow dashed, green dotted indicate A1, A2, A3. Right panel: Same as the left panel but for Group B, overlaid with A1 to A3 in grey lines. The upper panel shows the time evolution of the total energy in all CRs inside the SNR in units of the SN explosion energy $E_{\rm SN}$. Likewise the middle panel shows the evolution of the re-acceleration component. The lower panel shows the energy ratio between the re-acceleration component and the total. The figures are taken from [1].

To show the fractional contribution of re-acceleration to the accelerated CRs, Figure 2 displays snapshots of the accelerated proton spectra integrated over the whole SNR volume in certain selected ages. For a quantitative discussion, we also adopt the time evolution of the total kinetic energy from each CR component inside the SNR[1], i.e., $E_{\rm CR,re}$ for the kinetic energy in the re-acceleration component and $E_{\rm CR,fresh}$ in the freshly accelerated CR component respectively, which is shown in Figure 3. We calculate $E_{\rm CR,i}$ (where i = {re, fresh}) as

$$E_{\rm CR,i} = \int\int (\gamma - 1) m_{\rm p} c^2 f_{\rm i}(x,p) 4\pi p^2 dp d^3x \tag{2}$$

$$E_{\rm CR} = E_{\rm CR,re} + E_{\rm CR,fresh}, \tag{3}$$

[1]The escaped CRs are not included here since they do not contribute to the non-thermal emission from the remnant.

where γ is the Lorentz factor, $f(x, p)$ is the phase-space distribution function of the non-thermal particles. From Figure 2 and the top and middle panels of Figure 3, the flux of the re-acceleration component remains approximately constant from 1 $t_{\rm tr}$ to 3 $t_{\rm tr}$, whereas the flux of the freshly accelerated component decreases as the shock weakens and the injection and acceleration becomes inefficient, and is now dominated by the CRs accelerated in the past which is suffering from adiabatic loss.

As shown in the bottom panel of Figure 3, the ratio between the re-acceleration component and the total CR content increases with the SNR age up to a few $t_{\rm tr}$, indeed indicating an increasing importance of re-acceleration effect in older objects. However, the ratio increases only up to $\sim 35\%$ (A1 and A3) and $\sim 60\%$ (A2) by $3t_{\rm tr}$, which is far from a total domination used by the previous works. Admittedly these numbers should depend on parameters such as the ISM density, mass-loss history and so on as is shown by the differences between models A1 to A3, but our results clearly illustrate that it is important to account for the CR acceleration history coherently starting from the explosion itself in order to obtain an accurate estimation of the CR energy budget and spectra, and hence the non-thermal emission properties.

For a quick comparison, we also show the results from the models in Group B in the lower panel of Figure 3, and found the final ratio close to that predicted by model A2 (with the same $n_{\rm ISM} = 0.1$ cm^{-3}). In the young wind-interaction phase, the total (and fresh) component is roughly proportional to the pre-SN mass-loss rates, which can be understood as coming from the different masses in the gas swept up by the shock (and hence the number of particles injected into DSA) at any given age. On the other hand, re-acceleration component $E_{\rm CR,re}$ shows a much weaker dependence on the wind properties mainly due to the different nature of the seed particles involved, i.e., the pre-existing Galactic CRs whose density profile is assumed to be not affected by the mass loss. When the shock is still strong, propagating in the stellar wind, $E_{\rm CR}$ is mostly dominated by the freshly accelerated particles. This is quite different from the situation we expected for older SNRs which are often found to be interacting with dense molecular clouds and the shocks have already become radiative. In the latter case, $E_{\rm CR,re}$ is expected to play a much more important role than in the younger phase. At around a few 10^2 to 10^3 yrs, however, the ratio can reach around 1% for model B5, implying that re-acceleration of pre-existing CRs does contribute to the non-thermal emission for progenitors with smaller mass-loss rates.

As noted in the previous subsection, while it has been believed that the re-acceleration of Galactic CRs is sufficient to explain the non-thermal emission in older SNRs interacting with high density environments, our long-term simulation indicates that any CRs accelerated in the past before shock-cloud interaction cannot be ignored and should be treated self-consistently with the hydrodynamic evolution of the remnant from the explosion up to the current epoch, even though the shock has already become radiative now.

References

[1] Kobashi, R., Yasuda, H., & Lee, S.-H. 2022, ApJ, 936, 26

[2] Yasuda, H., Lee, S.-H., & Maeda, K. 2021, ApJL, 919, L16

[3] Yasuda, H., Lee, S.-H., & Maeda, K. 2022, ApJ, 925, 193

[4] Lee, S.-H., Slane, P. O., Ellison, D. C., et al. 2013, ApJ, 767, 20

[5] Slane, P., Lee, S.-H., Ellison, D. C., et al. 2014, ApJ, 783, 33

[6] Yasuda, H. & Lee, S.-H. 2019, ApJ, 876, 27

[7] Ackermann, M., Ajello, M., Allafort, A., et al. 2013, Sci, 339, 807

[8] Lee, S.-H., Patnaude, D. J., Raymond, J. C., et al. 2015, ApJ, 806, 71

[9] Uchiyama, Y., Blandford, R. D., Funk, S., et al. 2010, ApJL, 723, L122

[10] Malkov, M. A., Diamond, P. H., & Sagdeev, R. Z. 2011, NatCo, 2, 194

[11] Bykov, A. M., Malkov, M. A., Raymond, J. C., et al. 2013, SSRv, 178, 599

[12] Lee, S.-H., Ellison, D. C., & Nagataki, S. 2012, ApJ, 750, 156

[13] Blondin, J. M. & Ellison, D. C. 2001, ApJ, 560, 244

[14] Blasi, P. 2004, JKAS, 37, 483

[15] Caprioli, D., Amato, E., & Blasi, P. 2010, APh, 33, 307

[16] Caprioli, D., Kang, H., Vladimirov, A. E., et al. 2010, MNRAS, 407, 1773

[17] Sutherland, R. S. & Dopita, M. A. 1993, ApJS, 88, 253

[18] Townsend, R. H. D. 2009, ApJS, 181, 391

[19] Blondin, J. M., Wright, E. B., Borkowski, K. J., et al. 1998, ApJ, 500, 342

[20] Boulares, A. & Cox, D. P. 1990, ApJ, 365, 544

[21] Cox, D. P. 2005, ARA&A, 43, 337

[22] Noutsos, A. 2012, SSRv, 166, 307

[23] Hollenbach, D. & McKee, C. F. 1989, ApJ, 342, 306

[24] Crutcher, R. M. 1999, ApJ, 520, 706

[25] Martínez-Rodríguez, H., Badenes, C., Lee, S.-H., et al. 2018, ApJ, 865, 151

[26] Dwarkadas, V. V. & Chevalier, R. A. 1998, ApJ, 497, 807

[27] Patnaude, D. J., Lee, S.-H., Slane, P. O., et al. 2015, ApJ, 803, 101

[28] Heger, A. & Woosley, S. E. 2010, ApJ, 724, 341

[29] Truelove, J. K. & McKee, C. F. 1999, ApJS, 120, 299

[30] Matzner, C. D. & McKee, C. F. 1999, ApJ, 510, 379

[31] Cardillo, M. 2019, Galax, 7, 49